

Supporting Information

Morphology Controlled Lithium Storage in Li_3VO_4 Anode

Guang Yang,^{†ab} Bowei Zhang,^{†a} Jianyong Feng,^a Yu Lu,^a Zhiqiang Wang,^a Vanchiappan Aravindan,^{abd} Muthiah Aravind,^{ab} Jilei Liu,^{*c} Madhavi Srinivasan,^{*ab} Zexiang Shen^{abc} and Yizhong Huang^{*a}

^aSchool of Materials Science and Engineering, Nanyang Technological University, 639798, Singapore

^bEnergy Research Institute @ NTU (ERI@N), Nanyang Technological University, Research Techno Plaza, 50 Nanyang Drive, Singapore 637553

^cDivision of Physics and Applied Physics, School of Physical and Mathematical Sciences, Nanyang Technological University, 637371, Singapore

^dDepartment of Chemistry, Indian Institute of Science Education and Research (IISER), Tirupati-517507, India

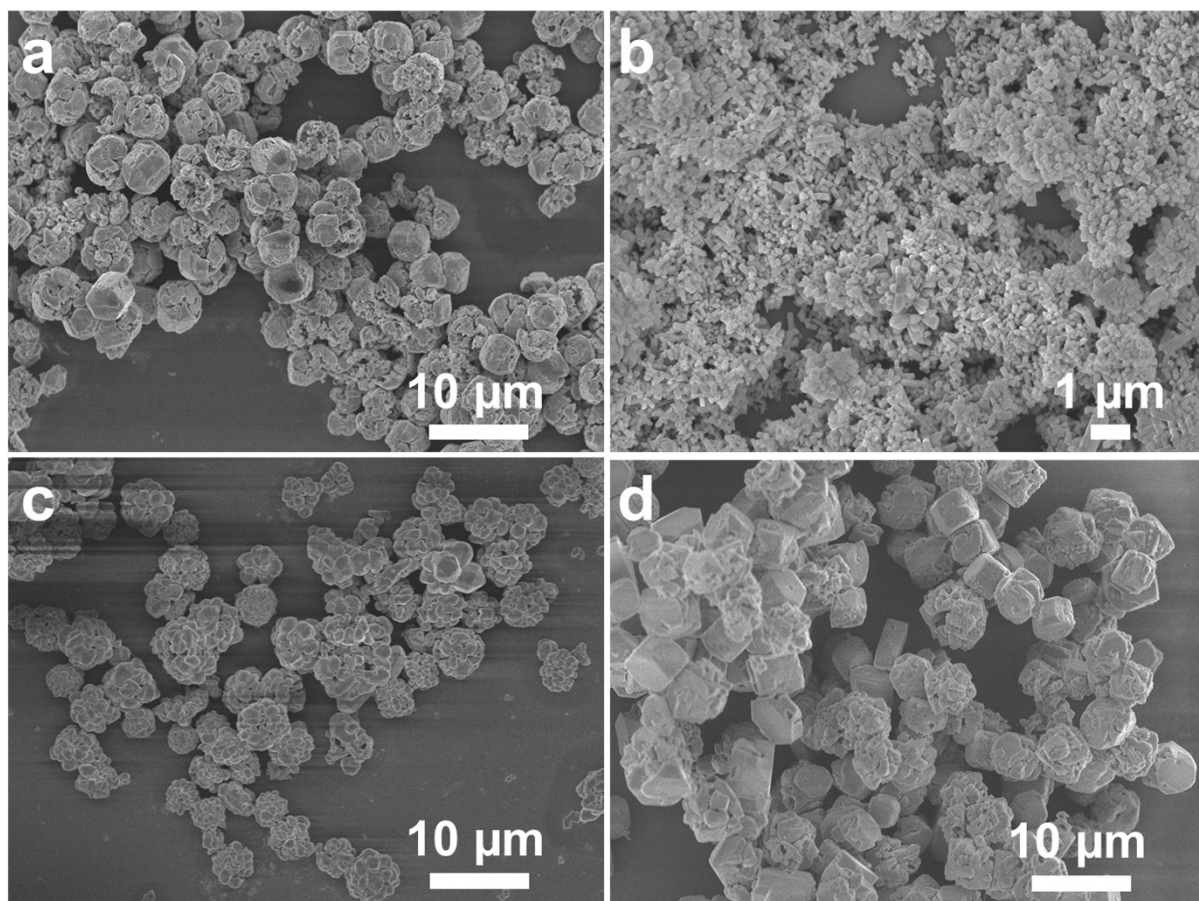


Fig. S1 SEM images of LVO of: (a) LVO-SPHERE, (b) LVO-ROD, (c) LVO-FLOWER, (d) LVO-BULK.

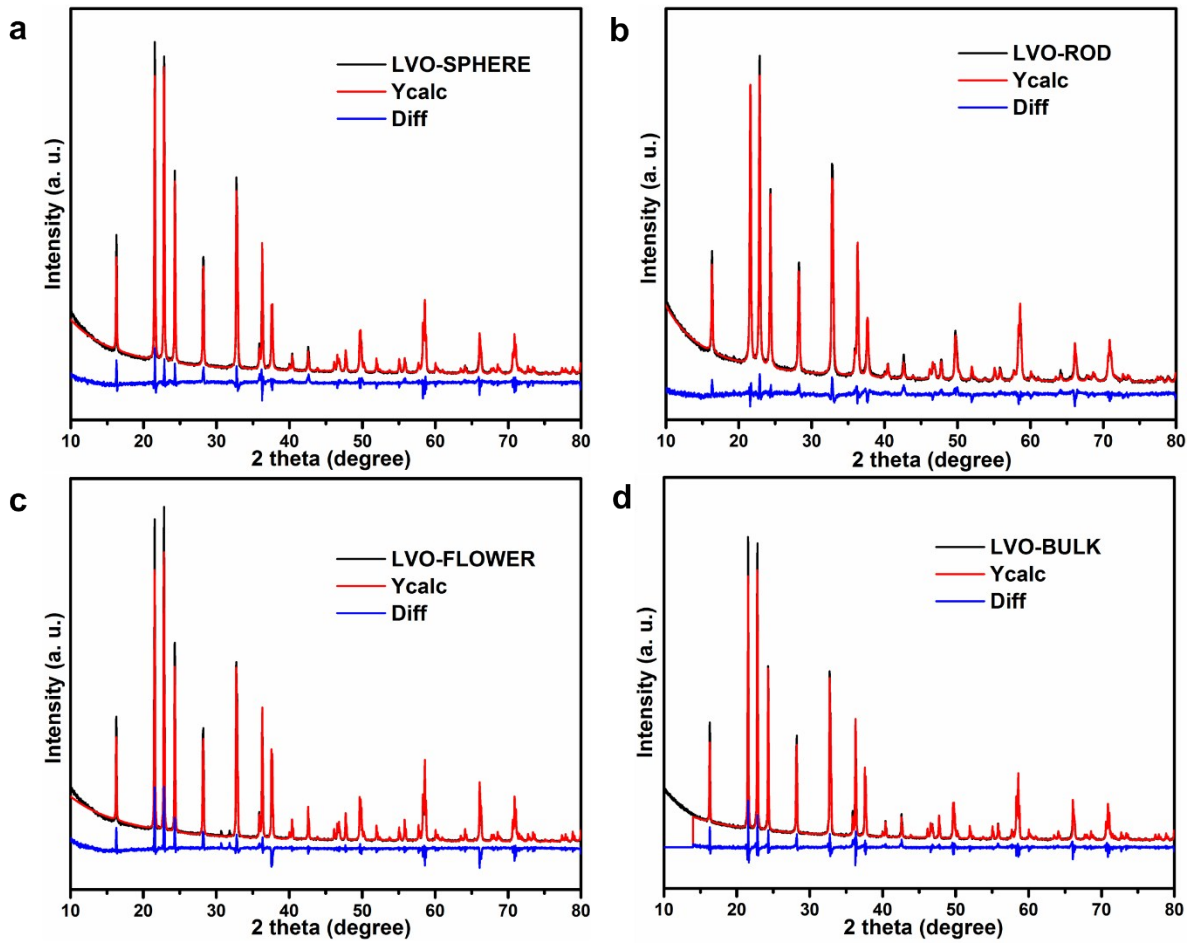


Fig. S2 Rietveld refinement of the XRD data for (a) LVO-SPHERE, (b) LVO-ROD, (c) LVO-FLOWER, (d) LVO-BULK.

Table S1. Lattice parameters of the samples

Sample	a(Å)	b(Å)	c(Å)	V(Å ³)	Rwp
LVO-SPHERE	6.3265376	5.4496384	4.9527315	170.75702	5.13
LVO-ROD	6.3268489	5.4523261	4.9571351	171.00155	2.86
LVO-FLOWER	6.32673	5.449300	4.950601	170.67820	7.78
LVO-BULK	6.3273897	5.4490063	4.9528472	170.76420	6.54

Table S2. FTIR peaks and their assignments.

Peaks	Band assignment	Reference
3433	$\nu(\text{OH})$ water	1
2344	CO ₂	2
1637	$\delta(\text{OH})$	1
1420	Amorphous carbon	1
851	$\nu_s(\text{V-O})$	3
806	$\nu_{as}(\text{V-O})$	3
466	$\nu_s(\text{V-O-V})$	1

ν : stretching; δ : bending.

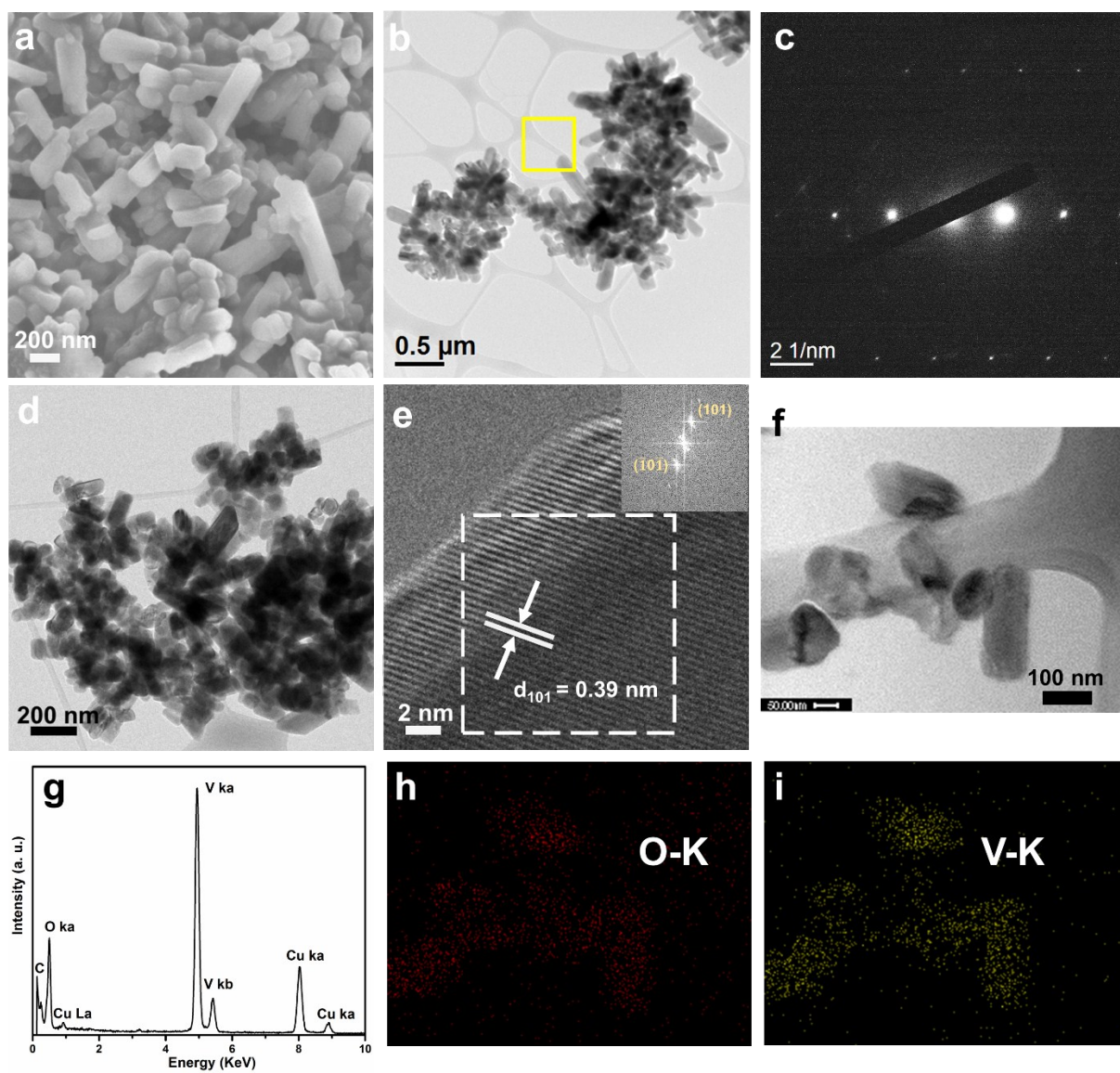


Fig. S3 (a) SEM and (b) TEM images of LVO-ROD, (c) SAED patterns from (b), (d-e) TEM and HRTEM of LVO-ROD, (f) TEM image of LVO-ROD, (g) EDX spectrum, and elemental mapping images of h) O and (i) V for LVO-ROD in (f).

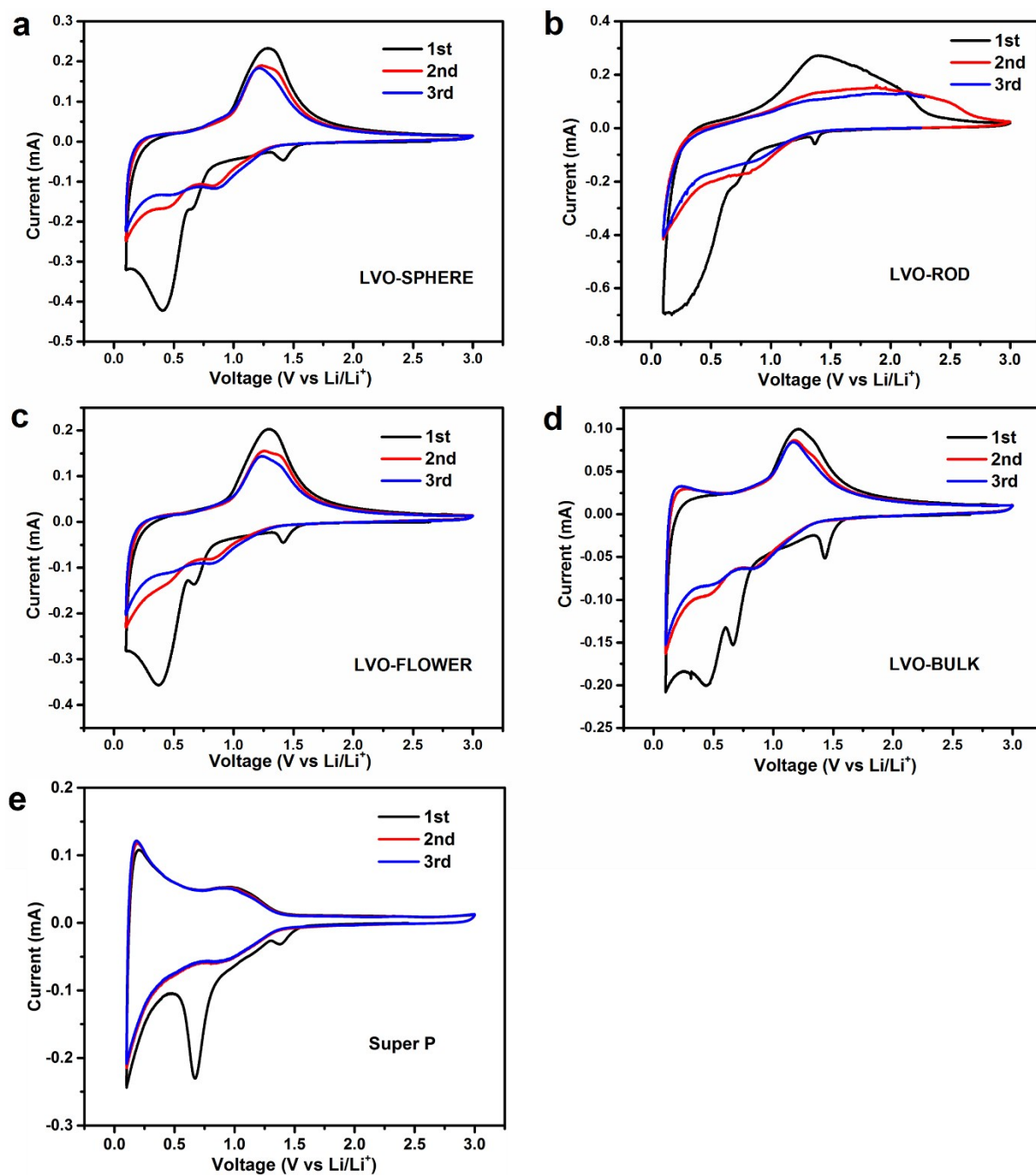


Fig. S4 First three CVs of: (a) LVO-SPHERE, (b) LVO-ROD, (c) LVO-FLOWER, (d) LVO-BULK, (e) Super P carbon additives with a scan rate of 0.2 mV s^{-1} in the voltage range of 0.1-3 V vs Li/Li⁺.

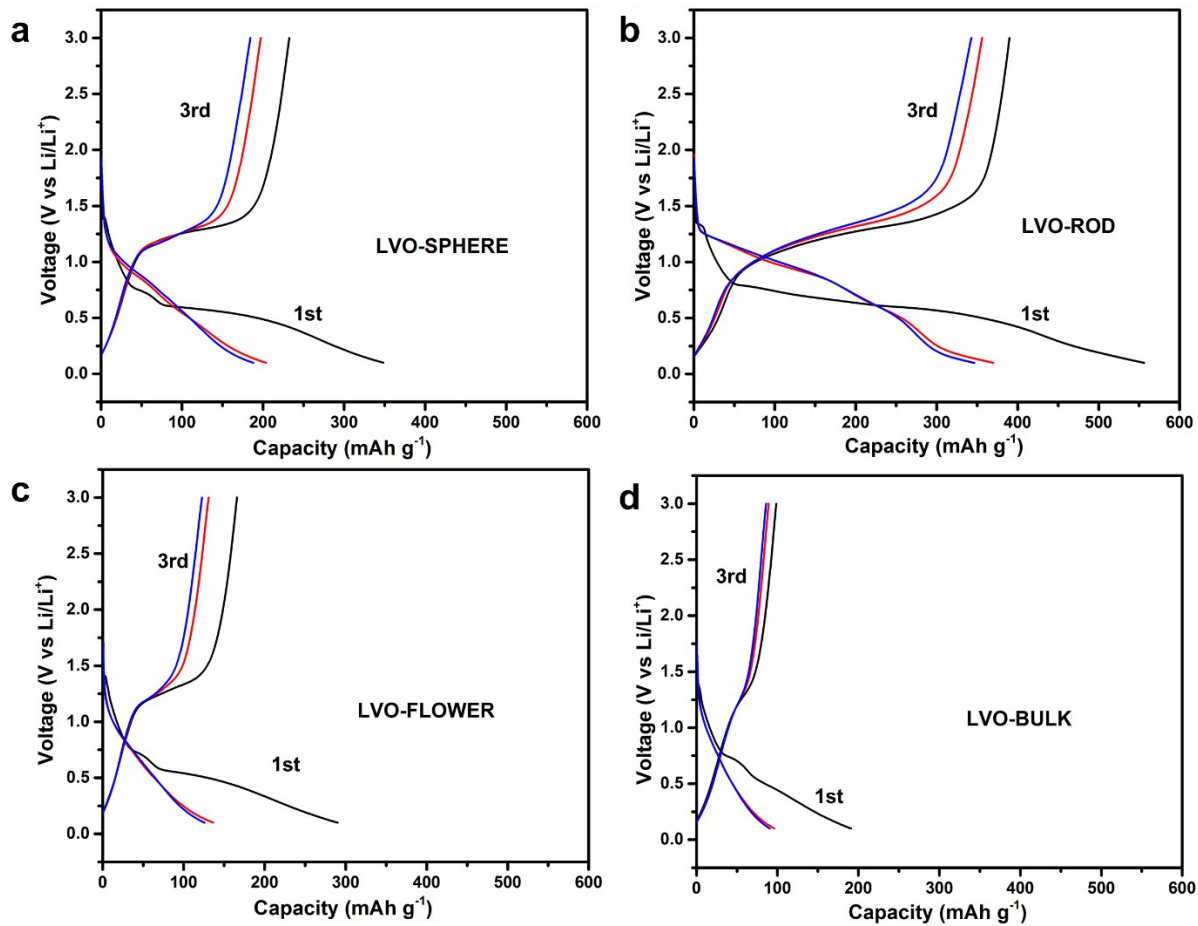


Fig. S5 First three galvanostatic discharge-charge profiles at a current rate of 0.1 A g^{-1} in the voltage range of $0.1\text{-}3 \text{ V vs Li/Li}^+$ for: (a) LVO-SPHERE, (b) LVO-ROD, (c) LVO-FLOWER, (d) LVO-BULK.

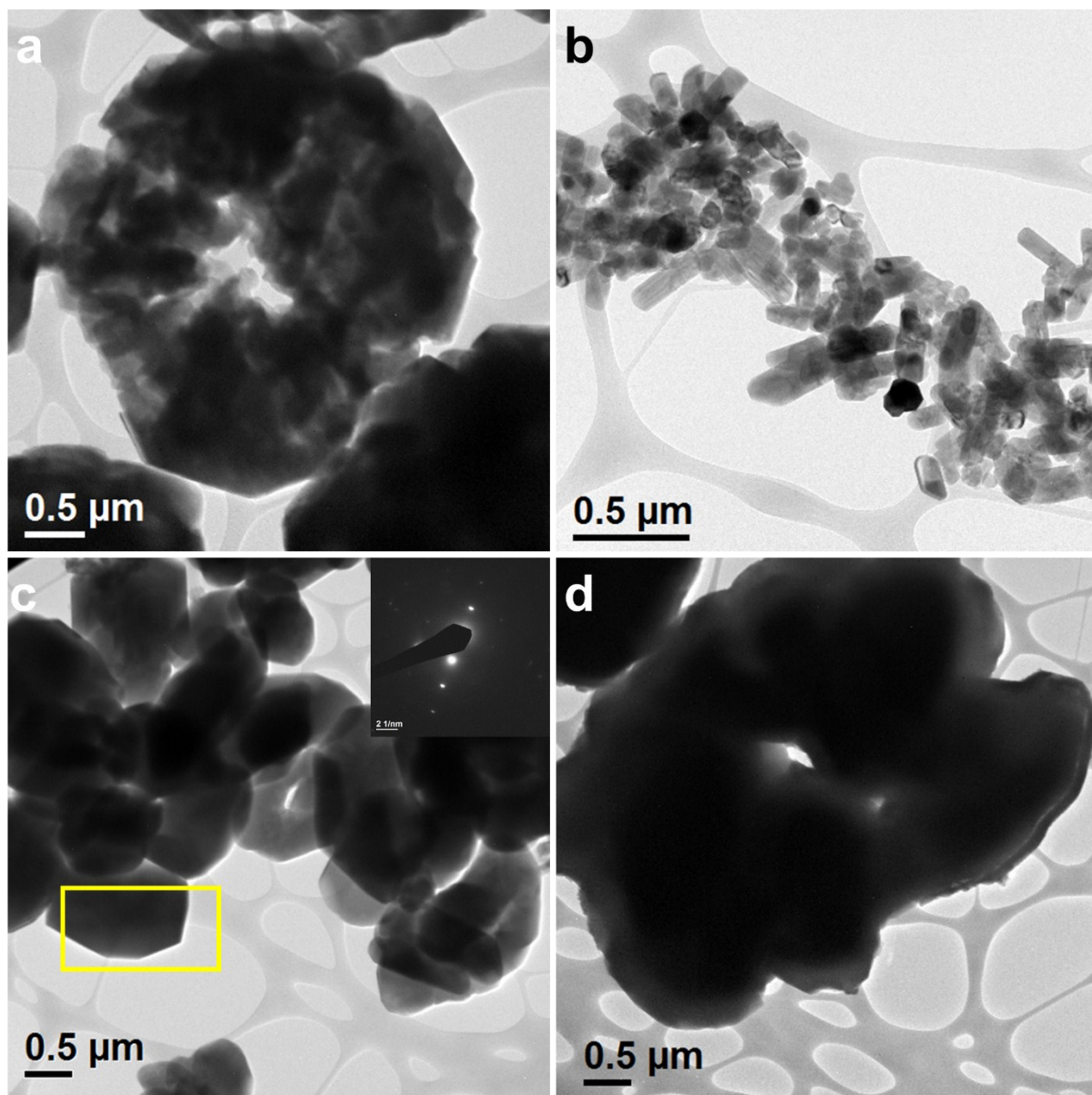


Fig. S6 TEM images of (a) LVO-SPHERE, (b) LVO-ROD, (c) LVO-FLOWER, (d) LVO-BULK.

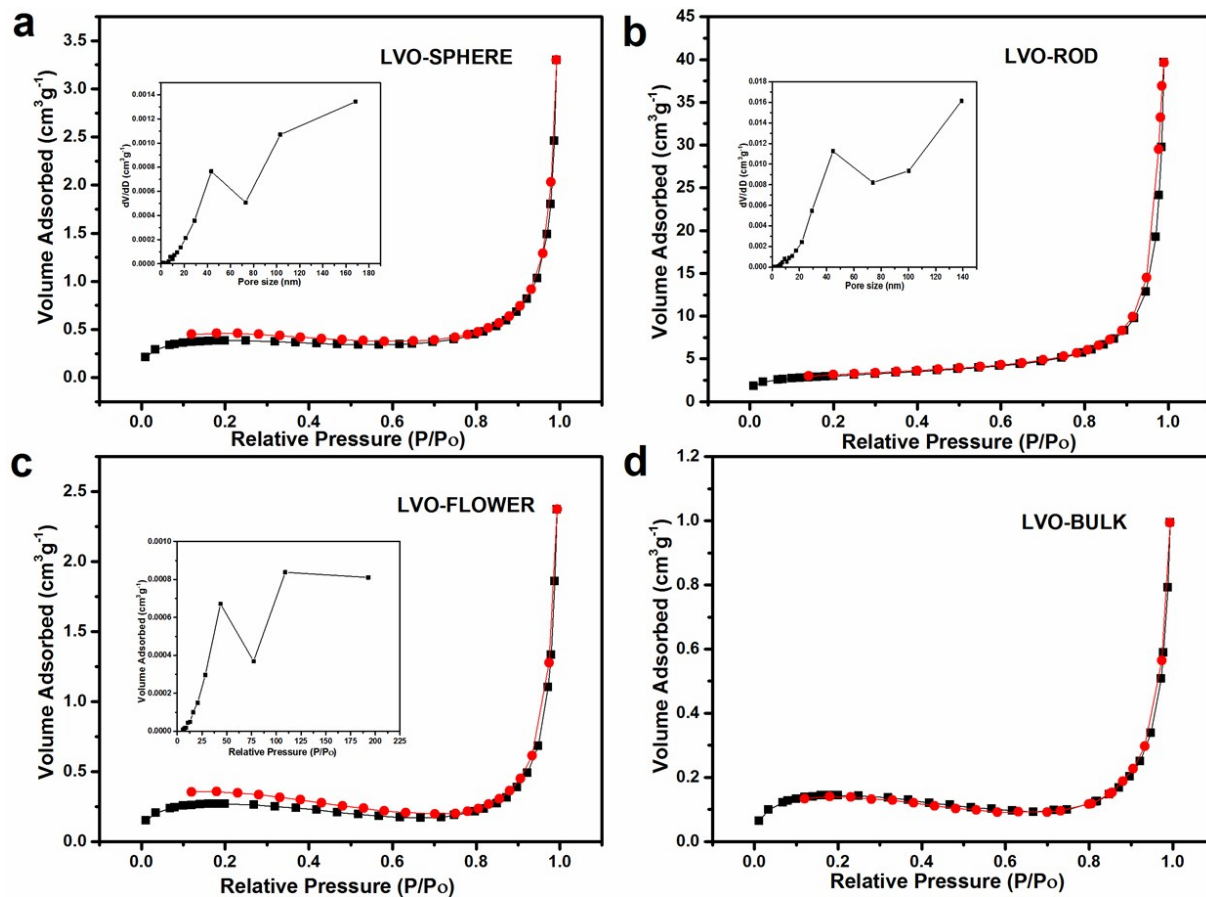


Fig. S7 N₂ adsorption-desorption isotherms of (a) LVO-SPHERE, (b) LVO-ROD, (c) LVO-FLOWER, (d) LVO-BULK.

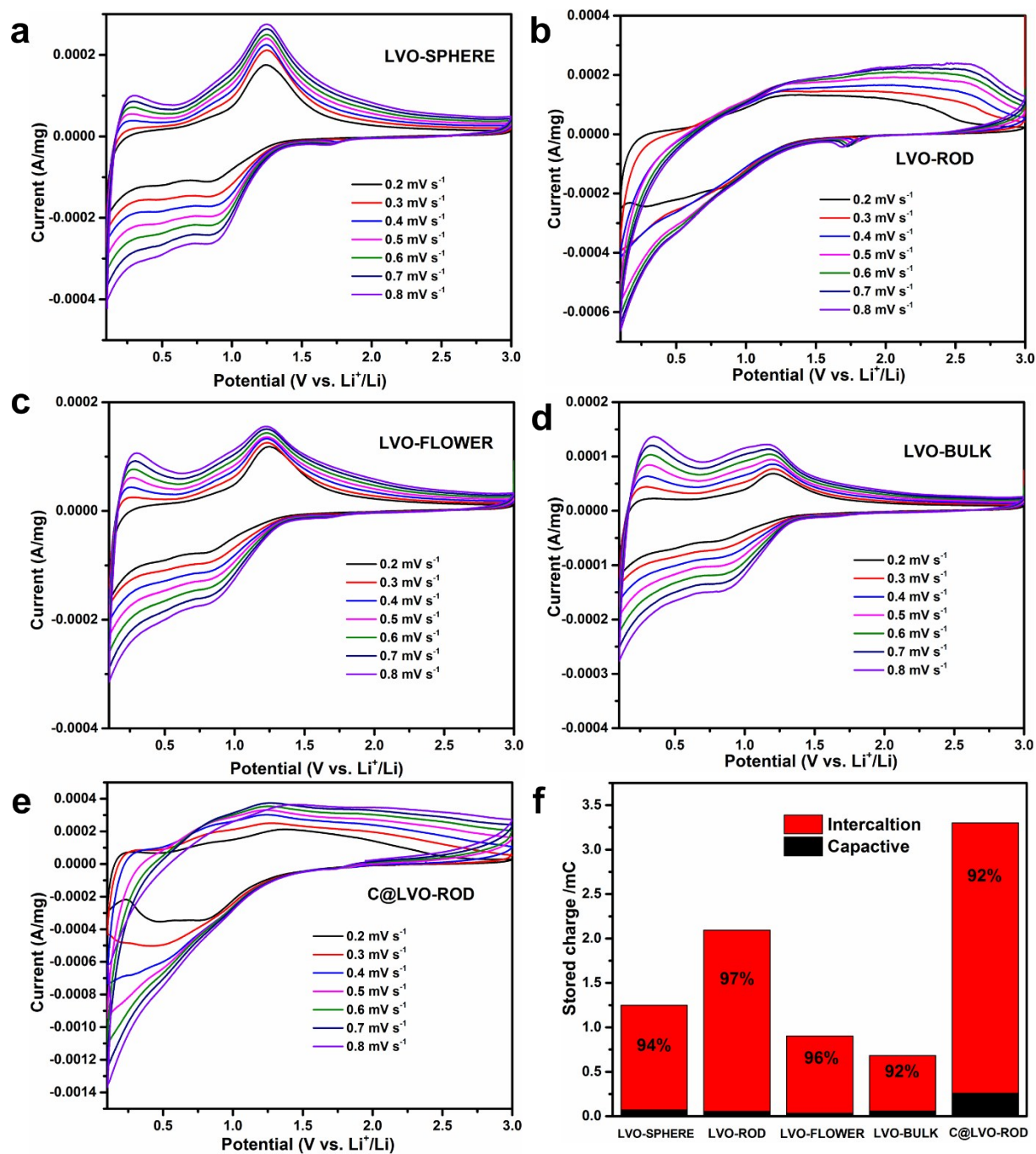


Fig. S8 CV curves of (a) LVO-SPHERE, (b) LVO-ROD, (c) LVO-FLOWER, (d) LVO-BULK, (e) C@LVO-ROD at different scan rates between 0.1 to 3V, (f) Dependence of oxidation peak current on the square root of scan rate for LVO-SPHERE, LVO-ROD, LVO-FLOWER, LVO-BULK and C@LVO-ROD; (f) Bar chart showing total stored charge with percentage contribution

from capacitive and intercalation at 0.2 mV/s for all the samples, the stored charge can be

$$Q = \int \left(\frac{i}{v} \right) dV \quad .4$$

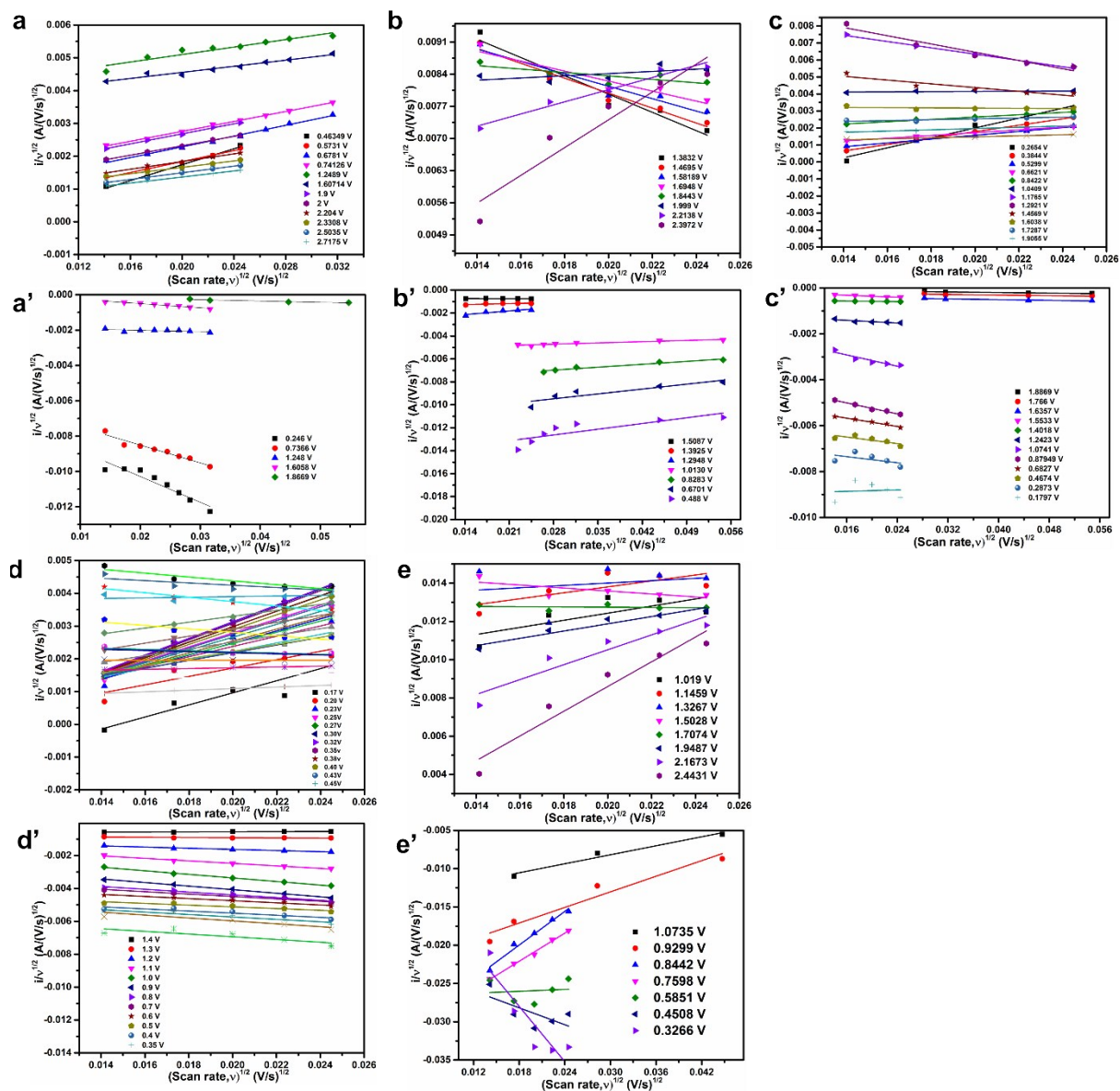


Fig. S9 (a, a'), (b, b'), (c, c'), (d, d') and (e, e') are the plots of $v^{1/2}$ vs $i/v^{1/2}$ for LVO-SPHERE, LVO-ROD, LVO-FLOWER, LVO-BULK, and C@LVO-ROD at both anodic and cathodic scan.

The plots are used for calculating constants K_1 and K_2 at different potentials of the cathodic scan and anodic scan.

The total current at a fixed potential can be described using the following equation:

$I(V) = K_1v + K_2v^{1/2}$, where K_1v and $K_2v^{1/2}$ represent the capacitive contribution and intercalation contribution, respectively. K_1 and k_2 can be obtained from the slope and y-axis intercept of the straight line: $i(V)/v^{1/2} = K_1v^{1/2} + K_2$, as shown in Fig. S9. Thus, the contribution from capacitive and intercalation can be calculated and each component contribution at scan rate of 0.2 mV/s is shown in Fig. S8f.5, 6

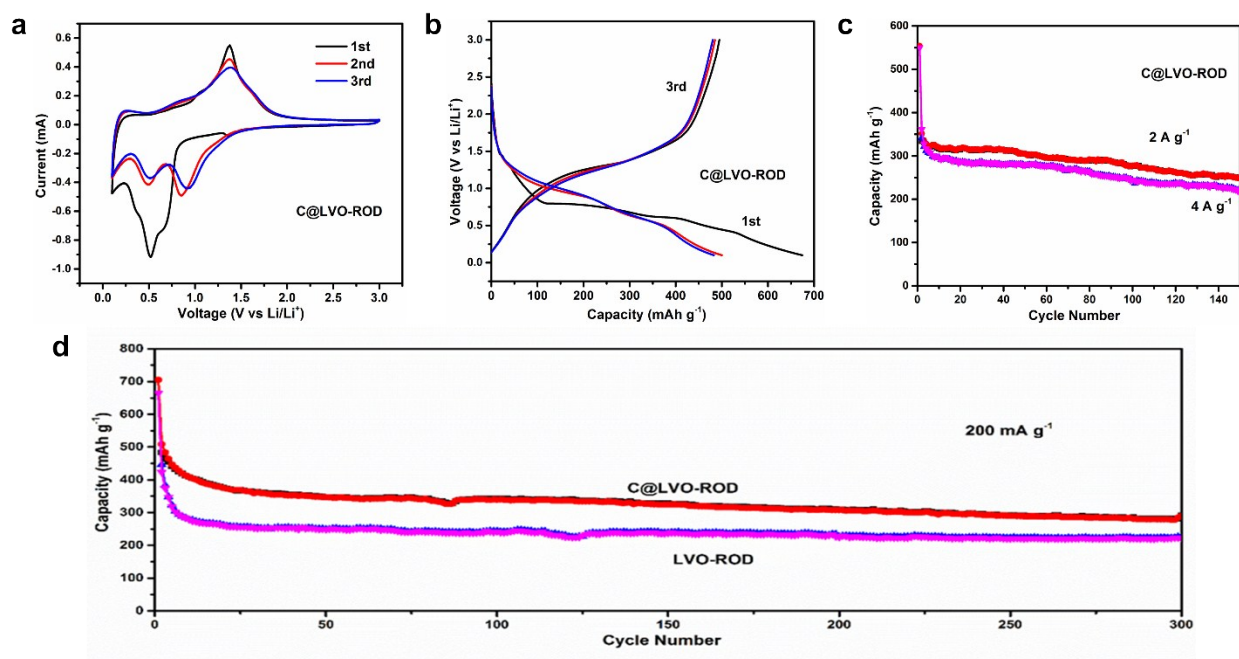


Fig. S10 (a) First three CV cycles of C@LVO-ROD, (b) Galvanostatic discharge-charge profiles of C@LVO-ROD for the first four cycles at a current rate of 0.1 A g⁻¹ in the voltage range of 0.1-

3.0 V vs Li/Li⁺, (c) Cycling performance of C@LVO-ROD at 2 and 4 A g⁻¹ for 150 cycles, (d) Cycling performance of C@LVO-ROD and LVO-ROD at 200 mA g⁻¹.

The electrochemical performance of C@LVO-ROD was examined and compared with LVO-ROD. Cyclic voltammetric (CV) curves measured are shown in Fig. S9a. In the first cathodic curve of C@LVO-ROD, three reduction peaks at around 0.75, 0.5 and 0.35 V are observed in the first cycle, which are attributed to the formation of solid-state interface (SEI) and the intercalation of Li⁺ into LVO. Shift of the reduction peaks to 0.5 and 0.8 V in the 2nd scan indicates the activation of the electrode material. The cathodic peaks of the first three cycles remain almost the same at around 1.35 V, which are correlated with delithiation process as similar to the previous reports.⁷⁻⁹ The 2nd cycle almost overlaps the 3rd CV cycles indicating the good cycling stability. The Fig. S9b shows the galvanostatic discharge-charge profiles where the first discharge capacity is 674 and the first charge capacity is 494, corresponding a first coulombic efficiency of 73.3%. The irreversible capacity is attributed to the solid electrolyte interface (SEI) film, which is consistent to the CV curves in Fig. S9a. It is worth to take note that the capacities of both subsequent discharge and charge cycles are almost consistent and reversible, compared to those of sample LVO-ROD (Fig. S9b).

Table S3. Summary of the electrochemical performance of Li₃VO₄ from literature.

Material	Current (mA g⁻¹)	Reversible capacity	Ref.
	1C ≈ 394 mA g⁻¹	mAh g⁻¹/cycle no.	
Li ₃ VO ₄	20 mA g ⁻¹	283/25	10
Li ₃ VO ₄	0.25 C	396/100	11
Li ₃ VO ₄ /C	1 C	394/100	7

Li ₃ VO ₄	0.2 C	164/100	12
		197/100	
Li ₃ VO ₄ /graphene	20 mA g ⁻¹	378/50	13
Li ₃ VO ₄ /C	0.8 C	363/40	14
Li ₃ VO ₄ /graphite	156 mA g ⁻¹	468/100	15
Li ₃ VO ₄ /CNTs	2000 mA g ⁻¹	250/2000	16
Li ₃ VO ₄ /graphene	0.2 C	453/200	17
Li ₃ VO ₄ /graphene	5 C	163/5000	18
Li ₃ VO ₄ /Ni	0.3 C	378/100	19
Li ₃ VO ₄ /C	20 mA g ⁻¹	245/50	20
Li ₃ VO ₄	0.1 C	311/50	21
Li ₃ VO ₄ /C	0.1 C	401/50	22
Li ₃ VO ₄ /C-Ni	1800 mA g ⁻¹	325/2000	23
Li ₃ VO ₄ /3D graphene	2 A g ⁻¹	Li ₃ VO ₄ /3D GN 356/200	24
		Li ₃ VO ₄ +3D GN 144/200	
Li ₃ VO ₄ /c	150 mA g ⁻¹	542/300	25
Li ₃ VO ₄ /N-C	150 mA g ⁻¹	544/800	26
Li ₃ VO ₄ /C	2 A g ⁻¹	280/500	27
Li ₃ VO ₄ /graphite	100 mA g ⁻¹	360/200	28
Li ₃ VO ₄ /C hollow sphere	800 mA g ⁻¹	LVO/C	29
		400/100	
		LVO 204/100	

Li ₃ VO ₄ /C/CNTs	4 A g ⁻¹	272/500	30
Li ₃ VO ₄ /C/rGO	2 A g ⁻¹	LVO/C/rGO 387/200 LVO/C 305/200	31
Li ₃ VO ₄ @C nanofiber	40 mA g ⁻¹	Fiber 394/100 Power 318/100	32
Mo ⁶⁺ doped Li ₃ VO ₄	2950 mA g ⁻¹	Mo ⁶⁺ -Li ₃ VO ₄ 439/200 Bare Li ₃ VO ₄ 166/200	33
Oxygen-deficient Li ₃ VO ₄	1 A g ⁻¹	244/500	9
C@ Li ₃ VO ₄ -ROD	100 mA g ⁻¹ 2 A g ⁻¹ 4 A g ⁻¹	430/100 250/150 220/150	This work

References

1. Q. Li, Q. Wei, J. Sheng, M. Yan, L. Zhou, W. Luo, R. Sun, L. Mai, *Adv. Sci*, 2015, **2**, 1500284.
2. P. Goel, M. Arora, *RSC Adv*, 2015, **5**, 29741-29747.
3. N.V. Kosova, D.O. Rezepova, A.B. Slobodyuk, *Electrochim. Acta*, 2015, **167**, 75-83.
4. P. Yu, C. Li, X. Guo, *J. Phys. Chem. C*, 2014, **118**, 10616-10624.
5. M. Sathiya, A.S. Prakash, K. Ramesha, J.M. Tarascon, A.K. Shukla, *J. Am. Chem. Soc*, 2011, **133**, 16291-16299.
6. J. Wang, J. Polleux, J. Lim, B. Dunn, *J. Phys. Chem. C*, 2007, **111**, 14925-14931.
7. Z. Liang, Z. Lin, Y. Zhao, Y. Dong, Q. Kuang, X. Lin, X. Liu, D. Yan, *J. Power Sources*, 2015, **274**, 345-354.

8. C. Zhang, C. Liu, X. Nan, H. Song, Y. Liu, C. Zhang, G. Cao, *ACS Appl. Mater. Interfaces*, 2015, **8**, 680-688.
9. K. Wang, C. Zhang, H. Fu, C. Liu, Z. Li, W. Ma, X. Lu, G. Cao, *Chem. Eur. J*, 2017, **23**, 5368–5374.
10. H. Li, X. Liu, T. Zhai, D. Li, H. Zhou, *Adv. Energy Mater*, 2013, **3**, 428-432.
11. S. Ni, X. Lv, J. Ma, X. Yang, L. Zhang, *J. Power Sources*, 2014, **248**, 122-129.
12. W.T. Kim, Y.U. Jeong, Y.J. Lee, Y.J. Kim, J.H. Song, *J. Power Sources*, 2013, **244**, 557-560.
13. Y. Shi, J.Z. Wang, S.L. Chou, D. Wexler, H.J. Li, K. Ozawa, H.K. Liu, Y.P. Wu, *Nano Lett*, 2013, **13**, 4715-4720.
14. Z. Liang, Y. Zhao, L. Ouyang, Y. Dong, Q. Kuang, X. Lin, X. Liu, D. Yan, *J. Power Sources*, 2014, **252**, 244-247.
15. S. Ni, X. Lv, J. Zhang, J. Ma, X. Yang, L. Zhang, *Electrochim. Acta*, 2014, **145**, 327-334.
16. Q. Li, J. Sheng, Q. Wei, Q. An, X. Wei, P. Zhang, L. Mai, *Nanoscale*, 2014, **6**, 11072-11077.
17. J. Liu, P.J. Lu, S. Liang, J. Liu, W. Wang, M. Lei, S. Tang, Q. Yang, *Nano Energy*, 2015, **12**, 709-724.
18. Z. Jian, M. Zheng, Y. Liang, X. Zhang, S. Gheyhani, Y. Lan, Y. Shi, Y. Yao, *Chem. Commun*, 2015, **51**, 229-231.
19. S. Ni, X. Lv, J. Ma, X. Yang, L. Zhang, *Electrochim. Acta*, 2014, **130**, 800-804.
20. G. Shao, L. Gan, Y. Ma, H. Li, T. Zhai, *J. Mater. Chem. A*, 2015, **3**, 11253-11260.
21. C. Du, J. Wu, J. Liu, M. Yang, Q. Xu, Z. Tang, X. Zhang, *Electrochim. Acta*, 2015, **152**, 473-479.
22. C. Zhang, H. Song, C. Liu, Y. Liu, C. Zhang, X. Nan, G. Cao, *Adv. Funct. Mater*, 2015, **25**, 3497-3504.
23. J. Zhang, S. Ni, T. Kang, J. Tang, X. Yang, L. Zhang, *J. Mater. Chem. A*, 2016, **4**, 14101-14105.
24. X. Jin, B. Lei, J. Wang, Z. Chen, K. Xie, F. Wu, *J. Alloys Compd*, 2016, **686**, 227-234.
25. S. Ni, J. Zhang, J. Ma, X. Yang, L. Zhang, X. Li, H. Zeng, *Adv. Mater. Interfaces*, 2016, **3**, 1500340.
26. J. Zhang, S. Ni, J. Ma, X. Yang, L. Zhang, *J. Power Sources*, 2016, **301**, 41-46.
27. P. Tartaj, J.M. Amarilla, M.B. Vazquez-Santos, *Chem. Mater*, 2016, **28**, 986-993.
28. S. Hu, Y. Song, S. Yuan, H. Liu, Q. Xu, Y. Wang, *J. Power Sources*, 2016, **303**, 333-339.
29. Y. Yang, J. Li, X. He, J. Wang, D. Sun, J. Zhao, *J. Mater. Chem, A*, 2016, **4**, 7165-7168.
30. Y. Yang, J. Li, D. Chen, J. Zhao, *J. Electrochem. Soc*, 2017, **164**, A6001-A6006.
31. Y. Yang, J. Li, J. Huang, J. Huang, J. Zeng, J. Zhao, *Electrochim. Acta*, 2017, **247**, 771-778.
32. R. Qin, G. Shao, J. Hou, Z. Zheng, T. Zhai, H. Li, *Sci. Bull*, 2017, **62**, 1081-1088.
33. Y. Dong, H. Duan, K.-s. Park, Y. Zhao, *ACS Appl. Mater. Interfaces*, 2017, **9**, 27688–27696.